A self-consistent integral equation study of the structure and thermodynamics of the penetrable sphere fluid

Cite as: J. Chem. Phys. **112**, 810 (2000); https://doi.org/10.1063/1.480649
Submitted: 26 August 1999 . Accepted: 13 October 1999 . Published Online: 29 December 1999

Maria-Jose Fernaud, Enrique Lomba, and Lloyd L. Lee

A self-consistent integral equation study of the structure and thermodynamics of the penetrable sphere fluid

Maria-Jose Fernaud and Enrique Lomba
Instituto de Química Física Rocasolano, CSIC, Serrano 119, E-28006 Madrid, Spain

Lloyd L. Lee
School of Chemical Engineering and Materials Science, University of Oklahoma, Norman, Oklahoma 73019-0628

(Received 26 August 1999; accepted 13 August 1999)

The penetrable sphere fluid consists of a system of spherical particles interacting via a potential that remains finite and constant for distances smaller than the particle diameter and is zero otherwise. This system, which was proposed sometime ago as a model for micelles in a solvent, has represented so far a remarkable challenge for integral equation theories which proved unable to correctly model the behavior of the two-body correlations inside the particle overlap region. It is shown in this work that enforcing the fulfillment of zero separation theorems for the cavity distribution function $y(r)$, and thermodynamic consistency conditions (fluctuation vs virial compressibility and Gibbs–Duhem relation), on a parametrized closure of the type proposed by Verlet, leads to an excellent agreement with simulation, both for the thermodynamics and the structure (inside and outside the particle core). Additionally, the behavior of the integral equation at high packing fractions is explored and the bridge functions extracted from simulation are compared with the predictions of the proposed integral equation. © *2000 American Institute of Physics.* [S0021-9606(00)51102-7]

I. INTRODUCTION

In recent years it has become clear that classes of materials such as solutions of certain types of colloidal particles—a particular example of what is nowadays known as ''soft matter''—can be modeled via ultrasoft potentials.[1] It is characteristic of this type of potentials that the excluded volume effects are relatively small, the particles being highly penetrable. This is the case of star polymer solutions for low arm numbers,[2,3] a system in which the dissolved polymer does not seem to undergo crystallization (''liquid–solid'' transition) for any concentration.

An extreme case, and perhaps the simplest, of ultrasoft potentials is the penetrable sphere model,[4] closely connected with Stillinger's Gaussian core model.[5] Both potentials illustrate what is known as bounded interactions, since they remain finite at zero separation. On the other hand, the ultrasoft potential recently proposed by Likos *et al.*[1] to model star polymer solution exhibits a logarithmic singularity at zero separation. The penetrable sphere model was first proposed by Marquest and Witten[4] to explain the crystallization of copolymer mesophases. On the basis of ground-state calculations, and the assumption of single-site occupancy, these authors concluded that an interaction of this type might give rise to a stable simple cubic phase in equilibrium with the fluid (i.e., with the disordered suspension of colloidal particles) in accordance with experimental evidence. More recently, however, a detailed study by Likos, Watzlawek, and Löwen[6] has shown that this is not the case when multiple site occupancy is allowed for, and thus one has to look for some other causes to explain the stability of the simple cubic phase, as for instance the influence of the many body interactions.

Nevertheless, Likos *et al.* have raised an important point in their study. It turns out that the integral equation approximations usually employed in the liquid state theory, like the Percus–Yevick (PY) equation, hypernetted chain approximation (HNC), or the Rogers–Young (RY) hybrid closure, either fail to reproduce the structure of the fluid (in particular for distances smaller than the particle size) or completely lack of a solution for many states of interest (from moderate to high concentrations of copolymer). In particular, in the case of the PY integral equation, this failure is easy to understand, since it is mostly suited for repulsive interactions, i.e., the larger the excluded volume region where the pair distribution function satisfies $g(r)=0$, the more accurate the approximation. However, the reason for the failure of the HNC is not so obvious. On the other hand, self-consistent approximations like the RY integral equation which interpolates between PY and HNC, in some cases either lack a solution or lead to disparate results, since as will be shown in this paper, consistency between virial and bulk compressibility turns out to be insufficient to guarantee a physically meaningful solution in systems in which the particle exclusion hardly plays any role.

From the above arguments it is clear that an integral equation that intends to describe the behavior of penetrable particles at small or zero separation will have to take into account some local consistency property of the functions describing the fluid structure at zero separation, going beyond simple thermodynamic consistency relations that are based on the use of quantities derived from the integration through-

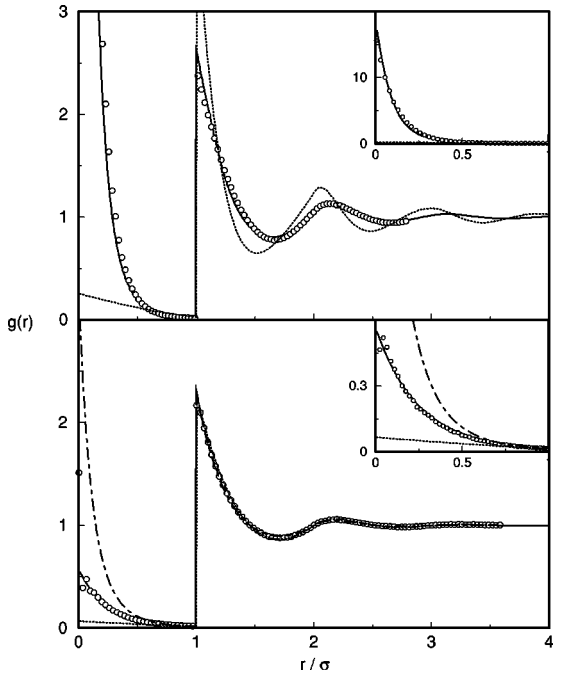

FIG. 1. Pair distribution function for the penetrable sphere fluid at $t=0.2$, $\eta=0.5$ (upper figure) and $\eta=0.3$ (lower figure). Monte Carlo results are denoted by empty circles, and integral equation approximations are represented by dashed–dotted (HNC), dotted (PY), and solid (ZSEP) curves.

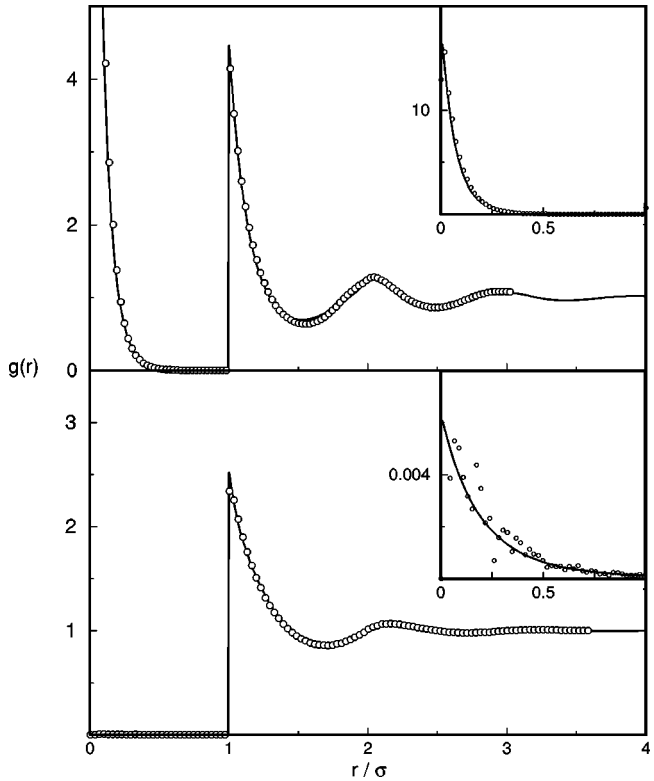

FIG. 2. Pair distribution function for the penetrable sphere fluid at $t=0.1$, $\eta=0.5$ (upper figure) and $\eta=0.3$ (lower figure). The strong statistical scattering of the MC data in the inset of the bottom part is due to the very low probability of penetration for such low temperatures and packing fractions which worsens the statistics of MC sampling in comparison with the other cases presented. Labels as in Fig. 1.

out the space of two-particle correlation functions. Precisely in order to take into account the correct behavior of the correlation functions inside the core region (even in systems with strong core repulsions), Lee[7] proposed some years ago a zero-separation (ZSEP) closure for the Ornstein–Zernike (OZ) integral equation which makes use of the zero separation limit of the cavity function $y(12)$ ($y(12)=\exp(\beta u(12))g(12)$, where $u(12)$ is the pair potential and $g(12)$ the pair distribution function) in addition to other thermodynamic consistency conditions. This ZSEP closure was explored in detail for Lennard-Jones systems by Lee, Ghonasgi, and Lomba[8] who showed that imposing the fulfillment of the zero-separation theorems for the cavity function in conjunction with the Gibbs–Duhem relation (chemical potential vs pressure) and the consistency between virial pressure and bulk compressibility leads to an excellent agreement for all correlation functions, including those like the cavity and bridge function which are non zero inside the overlap region. It is obvious that the ZSEP integral equation is an excellent candidate that by construction should be able to succeed where other approximations have failed. Thus, the main purpose of this work is to explore the ability of the ZSEP closure to describe the structural behavior and thermodynamics of the penetrable sphere fluid.

The rest of the paper is sketched as follows. In Sec. II we will summarize the essentials of the ZSEP integral equation, including the expressions for the calculation of the thermodynamic properties of interest. In Sec. III we will present our results as compared with simulation data. We also draw conclusions that are deemed significant and give future perspectives.

II. THE ZSEP INTEGRAL EQUATION

Once again, the starting point of our discussion will be the single-component OZ equation,

$$h(r_{12})=c(r_{12})+\rho\int c(r_{13})h(r_{32})d\mathbf{r}_3, \tag{1}$$

where $c(r)$ is the direct correlation function, $h(r)=g(r)-1$ is the total correlation function, and ρ is the number density of the polymer particles. The ZSEP approximation[9,10] assumes a closure relation of the form proposed by Verlet,[11]

$$g(r)=\exp[-\beta u(r)+h(r)-c(r)+B_{\mathrm{ZSEP}}(r)], \tag{2}$$

with

$$\hat{B}_{\mathrm{ZSEP}}(\gamma^*)=-\frac{\zeta\gamma^*(r)^2}{2}\left[1-\frac{\alpha\phi\gamma^*(r)}{1+\alpha\gamma^*(r)}\right], \tag{3}$$

where, for the penetrable sphere model

$$u(r)=\begin{cases}\varepsilon, & r\leqslant\sigma\\ 0, & r>\sigma\end{cases}. \tag{4}$$

Here σ is particle size and $\varepsilon>0$. The function $\gamma^*(r)=\gamma(r)+\frac{1}{2}\rho[\exp(-\beta u^r_{wca}(r{:}\sigma_{wca})-1]$ and $\gamma(r)=h(r)-c(r)$ represents indirect correlations in the fluid. The renormalization potential is defined by

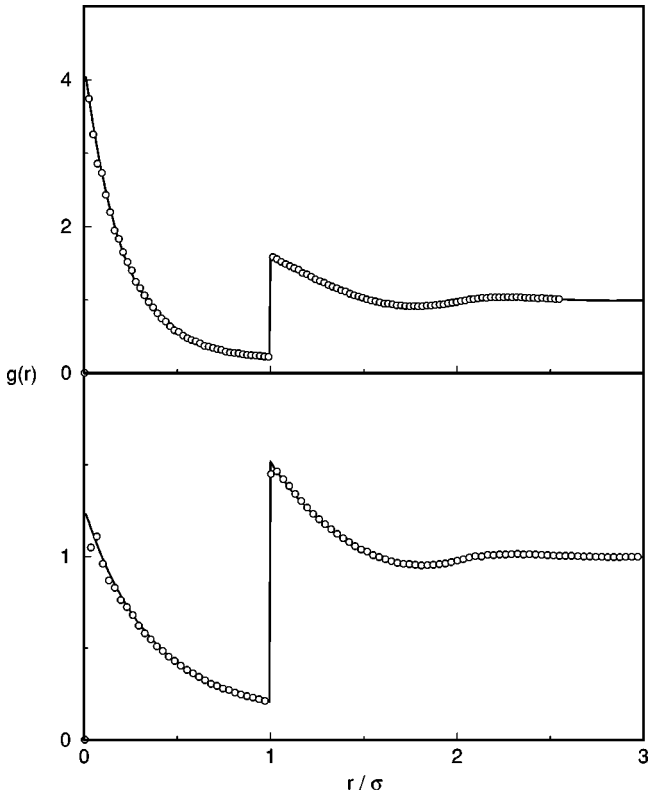

FIG. 3. Pair distribution function for the penetrable sphere fluid at $t=0.5$, $\eta=0.5$ (upper figure) and $\eta=0.3$ (lower figure). Labels as in Fig. 1.

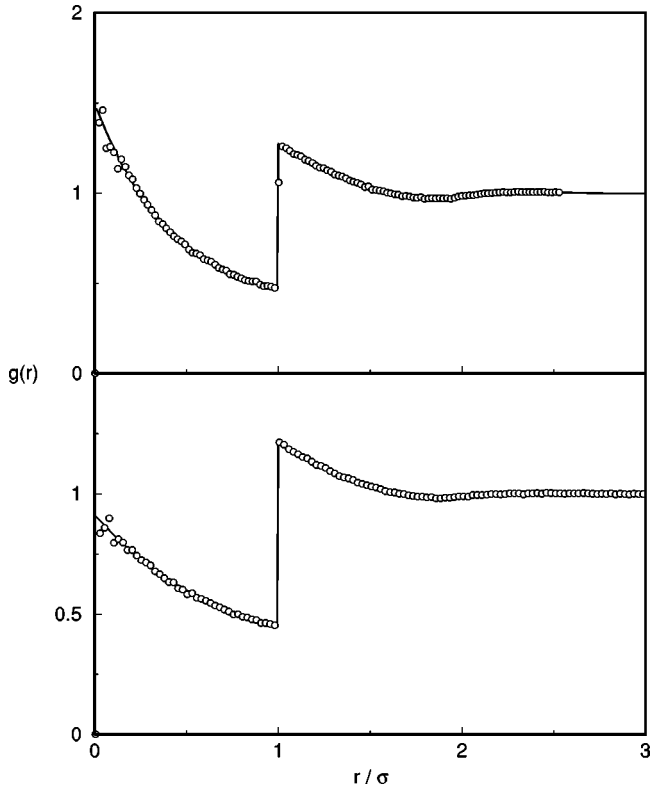

FIG. 4. Pair distribution function for the penetrable sphere fluid at $t=1.0$, $\eta=0.5$ (upper figure) and $\eta=0.3$ (lower figure). Labels as in Fig. 1.

$$\beta u^r_{wca}(r) = \begin{cases} 4((\sigma_{wca}/r)^{12}-(\sigma_{wca}/r)^6)+1 & \text{if } r<2^{1/6}\sigma_{wca} \\ 0 & \text{if } r>2^{1/6}\sigma_{wca} \end{cases}.$$

The diameter σ_{wca} can be used as an optimization parameter in addition to ζ, ϕ, and α in (3), though in most cases one can use the value that, in a system interacting via u^r_{wca}, would render the same second virial coefficient as in the penetrable sphere fluid at the same density.

This form of the renormalized indirect correlation function, γ^*, differs from the one proposed in (8) and (9) in the ρ-dependence that guarantees the correct low density limit—in the spirit of the approximation also proposed by Duh and Henderson[12]—of the bridge function. Also, we have found that the subtraction of the Mayer bond leads to a better renormalization for repulsive potentials where the perturbative splitting of Refs. 9 and 10 is inadequate. Now, in the closure (2)–(3) we have three parameters ζ, ϕ and α (four if σ_{wca} is included in the optimization) that will have to be determined via consistency conditions as follows.

A. Virial pressure vs bulk compressibility (fluctuation theorem)

As usual, the virial pressure is given by

$$\beta P^v = \rho - \frac{2\pi}{3}\rho^2 \int g(r)\frac{\partial(\beta u(r))}{\partial r} r^3\, dr \tag{5}$$

which in this case reduces to

$$\beta P^v = \rho + \frac{2\pi}{3}\rho^2[g(\sigma^+)-g(\sigma^-)], \tag{6}$$

where $g(\sigma^{\pm})$ are the upper and lower limits of $g(r)$ at the core discontinuity. Also, the inverse isothermal compressibility via the fluctuation theorem reads

$$1/\kappa^f_T = \left(\frac{\partial \beta P}{\partial \rho}\right) = \left[1+4\pi\rho\int_0^\infty r^2 h(r)\,dr\right]^{-1}. \tag{7}$$

Hence a first consistency requirement will be

$$1/\kappa^f_T = \left(\frac{\partial \beta P^v}{\partial \rho}\right) = 1/\kappa^v_T. \tag{8}$$

B. Gibbs–Duhem relation

This is the thermodynamic relation that establishes the link between pressure, chemical potential, and density. In our case we will require that the virial pressure satisfy

$$\left(\frac{\partial P^v}{\partial \mu}\right)_T = \rho. \tag{9}$$

In order to avoid cumbersome thermodynamic integrations, one should have a direct expression for the excess chemical potential which in the case of the ZSEP closure (2)–(3), can simply be evaluated via Lee's star function approach,[7] which leads to[8]

$$\beta\mu' = \rho\int [\ln y(r) - h(r) + \tfrac{1}{2}h(r)\gamma(r) + h(r)B(r)]d\mathbf{r} - S^\star, \tag{10}$$

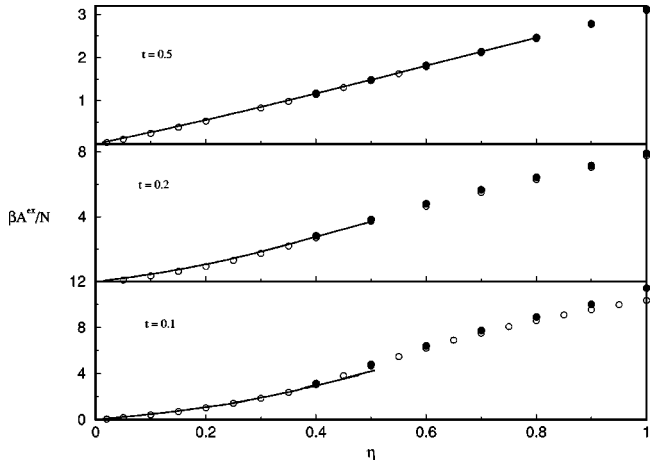

FIG. 5. Excess free energy per particle obtained from the ZSEP integral equation (solid lines) and from simulation via the η-route (empty circles) and the t-route (filled circles) taken from Ref. 6.

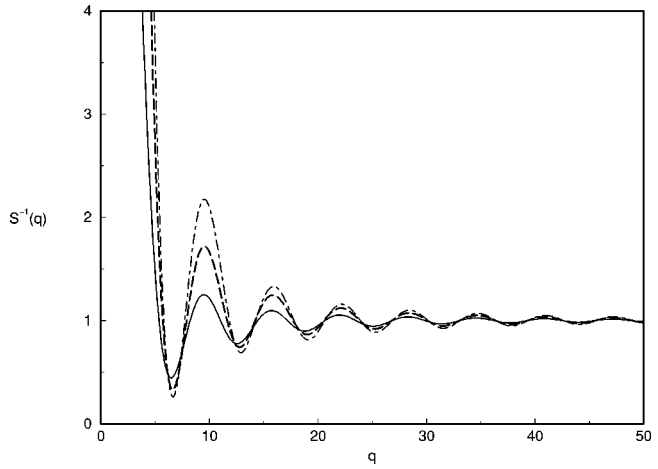

FIG. 7. Inverse of the structure factor of the penetrable sphere fluid at $t=0.2$, $\eta=0.5$ (solid curve), $\eta=0.7$ (dotted curve) and $\eta=0.9$ (dashed–dotted curve).

where the star series $S^{\star}$ is given by

$$S^{\star}=\rho\int d\mathbf{r}\frac{h(r)}{\gamma(r)}\int_{\gamma^{*}(0)}^{\gamma^{*}(1)}dx\,\hat{B}(x) \tag{11}$$

In the present case $\gamma^{*}(1)=\gamma^{*}$ and $\gamma^{*}(0)=\rho(\exp(-\beta u_{wca})-1)/2$, and the integral of the bridge function is given analytically by

$$\int_0^x ds\,\hat{B}(s)=-\frac{\zeta(\alpha x)^3}{6\alpha^3}+\frac{\zeta\phi}{6\alpha^3}\left[(1+\alpha x)^3-\frac{9}{2}(1+\alpha x)^2+9(1+\alpha x)-3\ln(1+\alpha x)-\frac{11}{2}\right]. \tag{12}$$

We see that, once all the correlation functions are known, we can determine the chemical potential and check for the fulfillment of the Gibbs–Duhem relation.

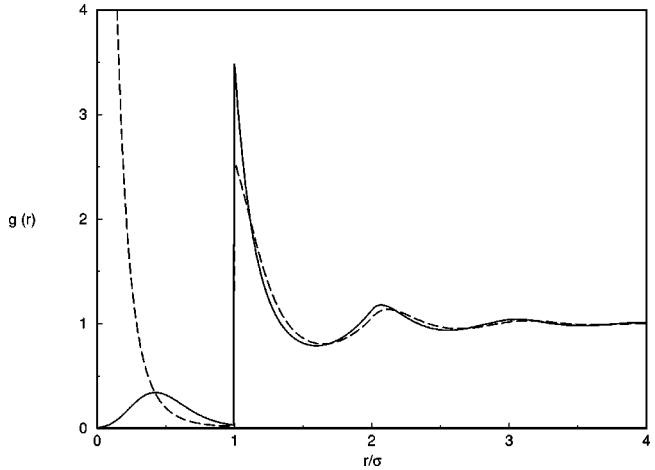

FIG. 6. Two solutions of the OZ equation with self-consistent closure at $t=0.2$ and $\eta=0.5$. The solid curve represents a solution that fulfills the Gibbs–Duhem and the virial-fluctuation theorem consistency conditions only. The dashed curve complies additionally with the zero separation theorem.

C. Zero separation theorems for the cavity function

In general, the value of the cavity distribution function $y(r)$ at a given distance $r=R$, can be shown to be identical to the energy required to insert a dimer of two particles separated a distance R minus the work required to independently insert two monomers. The latter quantity is simply twice the chemical potential. In particular, for $R=0$, we will have

$$-\ln y(0)=\beta\mu_2'(0)-2\beta\mu_1', \tag{13}$$

where $\beta\mu_1'$ can be obtained via Eqs. (10)–(12), and for $\beta\mu_2'(0)$ we have to write the corresponding OZ equations for the mixture of monomers and an infinitely diluted dimer (i.e., $\rho_2\to 0$) which reads

$$\begin{aligned}\tilde{h}_{11}&=\tilde{c}_{11}+\rho_1\tilde{h}_{11}\tilde{c}_{11},\\ \tilde{h}_{12}&=\tilde{c}_{12}+\rho_1\tilde{h}_{11}\tilde{c}_{12},\end{aligned} \tag{14}$$

where the tildes denotes a Fourier transformation, ρ_1 stands for the fluid density, $h_{11}=h(r)$ ($c_{11}=c(r)$) is the fluid total (direct) correlation function, and the subscripts 12 refer to

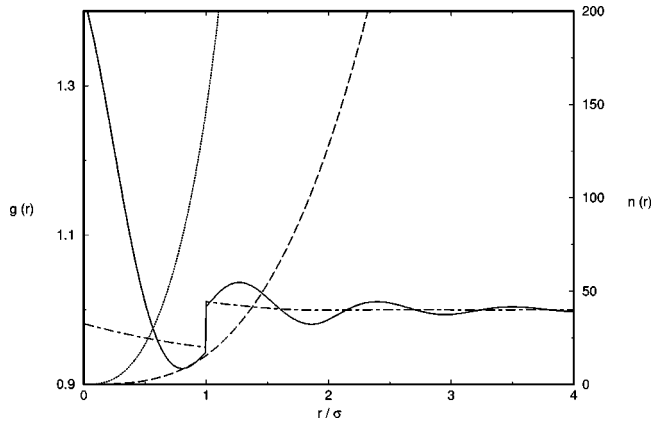

FIG. 8. Pair correlation function and coordination number, $n(r)$ (ordinates on the right axis) in the ZSEP approximation at extremely high densities. The solid (dashed) line corresponds to $g(r)$ ($n(r)$) at $\eta=12$ and the dotted–dashed (dotted) to $g(r)$ ($n(r)$) at $\eta=2$ and $t=16$ in both cases.

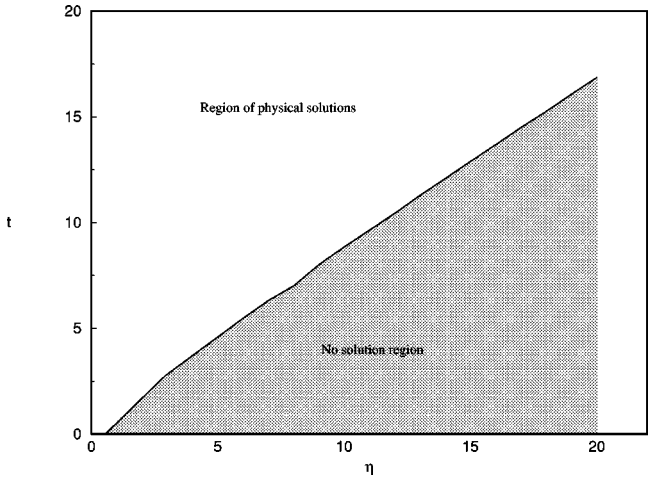

FIG. 9. Region of accessible solutions for the ZSEP integral equation.

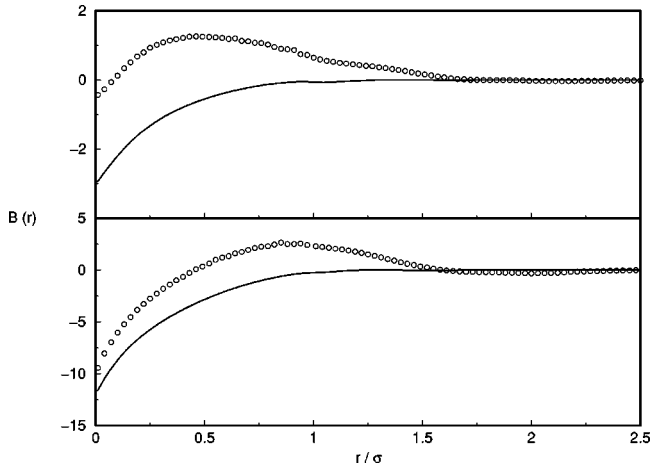

FIG. 10. Bridge functions extracted from the simulation data (empty circles) and compared with the ZSEP approximation (solid curves) for $\eta=0.5$, $t=0.2$ (upper figure) and $t=0.1$ (lower figure).

fluid-dimer correlations. Thus, once the bulk fluid structure is known (with some initial guess for ζ,ϕ, and α), h_{11} and c_{11} are inserted in (14), which is then solved in conjunction with ZSEP closure (2)–(3). Notice however that now $u_{12}(r)=2u_{11}(r)$, so in principle one should use a different set of ζ,ϕ, and α for the monomer-dimer bridge function, which should be consistent with those that would be obtained for the bulk fluid at a new reduced temperature $t'=(t/2)(t=k_BT/\varepsilon)$. In practice we have found that the results are sufficiently good using the same set of parameters for the dimer as for the bulk fluid integral equations and all the calculations in this work make use of this approximation.

Finally, the dimer chemical potential can also be evaluated via the star series

$$\beta\mu_2'=\rho_1\int\left[\ln y_{12}(r)-h_{12}(r)+\tfrac{1}{2}h_{12}(r)\gamma_{12}(r)+h_{12}(r)B_{12}(r)\right]d\mathbf{r}-S_{12}^{\star} \tag{15}$$

and with $S_{12}^{\star}$ defined by Eqs. (10)–(12) using fluid-dimer correlation functions instead.

Now we proceed as follows. For a set of initial parameters ζ,ϕ, and α, one solves the OZ equation (1) with the ZSEP closure (2)–(3). Then one calculates the virial pressure and the bulk compressibility. In order to estimate κ_T^v one simply has to solve the equation for three consecutive densities $(\rho,\rho\pm d\rho)$ and compute the numerical derivative. The chemical potential is obtained via Eqs. (10)–(12) and the values obtained for $(\rho,\rho\pm d\rho)$ are employed to estimate the density from the Gibbs–Duhem relation,

$$\rho^{\mathrm{GD}}=\left(\frac{\partial P}{\partial\mu}\right)_T$$

using a three point rule. This estimate should match the input number density, ρ. Then one solves the equations for the infinitely diluted dimer (14) and obtains $\beta\mu_2'$ and the zero-separation value, $y(0)$ from Eq. (13), which is to be compared with

$$\ln y_{cr}(0)=h(0)-c(0)+B_{\mathrm{ZSEP}}(0).$$

In principle one should vary ζ,α, and ϕ (and in some cases σ_{wca}) until a satisfactory agreement is reached for all this quantities. However, in the process of search for consistency it might well happen that complete consistency is never achieved, for instance if the functional form of $B(r)$ is not flexible enough to model the behavior of the fluid through changes in the independent parameters. We have therefore decided to look for the parameters that minimize an ''inconsistency residue,'' Φ_R, defined by

$$\Phi_R=\sqrt{w_P[1/\kappa_T^f-1/\kappa_T^v]^2+w_\rho[\rho-\rho^{\mathrm{GD}}]^2+w_z[\ln y(0)-\ln y_{cr}(0)]^2}, \tag{16}$$

where w_P,w_ρ,w_z are weights to be tuned in order to maximize the contribution of those conditions that might have the most influence on the quality of the results. More explicitly, we have used w_P, w_ρ, $w_z=1$, 2, 2, since at high densities we have found that the deviations in the compressibility consistency are unavoidably large and would otherwise mask departures in the remaining contributions. A direct search complex algorithm has been applied to locate the minima of Eq. (16), since this problem is too unstable for application of the faster but less robust Newton–Raphson or conjugate gradient algorithms.

Finally, note that the excess free energy per particle, βa^{ex} can also be calculated using

$$\beta a^{\mathrm{ex}}=\beta\mu_1'-\beta P/\rho+1$$

giving an alternative path to calculate the pressure,

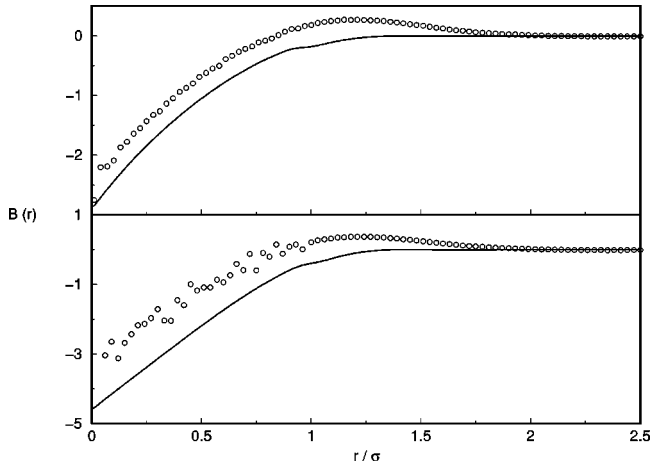

FIG. 11. Bridge functions extracted from the simulation data (empty circles) and compared with the ZSEP approximation (solid curves) for $\eta=0.3$, $t=0.2$ (upper figure) and $t=0.1$ (lower figure).

$$\frac{\beta P}{\rho}=1+\rho\left(\frac{\partial \beta a^{\mathrm{ex}}}{\partial \rho}\right). \tag{17}$$

III. RESULTS AND CONCLUSIONS

We have solved the ZSEP integral equation for a variety of states for which we have simulation data available. First, in Fig. 1 we compare the structure obtained from the ZSEP equation with the PY and HNC results and the simulation data. Notice that for the packing fraction $\eta=\pi\rho\sigma^3/6=0.5$ the HNC lacks physical solutions. One can clearly appreciate that the ZSEP closure agrees extraordinarily well with the simulation results in particular for the overlap region. The same can be seen in Figs. 2–4, where the correlation functions are shown for other packing fractions and temperatures. Also, in Fig.5 the ZSEP excess free energy in the liquid is compared with that obtained from the simulation. We can see once again that for the temperatures and packing fractions considered the agreement is remarkable.

It is important to note how the zero-separation theorem plays a crucial role to drive the optimization procedure towards physically meaningful solutions at high densities. This is illustrated in Fig. 6, where we show a solution obtained setting $w_z=0$ in Φ_R—in Eq. (16)—and the solution converged with $w_z=2$. One observes that relaxing the zero separation condition leads to a solution that is found to be incorrect, although fulfills the Gibbs–Duhem relation and the compressibility consistency condition. However, these quantities being either integrated properties or dependent on the value of the correlation functions at the core discontinuity, compliance with the corresponding consistency constraints does not guarantee the proper behavior at $r=0$. This would certainly not be the case when the hard sphere limit was approached ($\varepsilon\to\infty$), since there the core condition: $g(r)=0$ for $r<\sigma$ would be exactly fulfilled and the local behavior at contact $g(\sigma^+)$ would be made consistent with the integrated properties (both κ_T and $\beta\mu$). For a given t, the integral equation finally reaches a limiting η where convergence stops. In Fig. 7 we have plotted the quantity $1-\rho\tilde{c}(q)=S(q)^{-1}$ for various packing fractions approaching this limit at $t=0.2$. It is clear that the condition $S(q_0)^{-1}\to 0$ for $q_0\neq 0$ (i.e., the signature of a spatially ordered phase) is not even approached. Hence we cannot attribute the convergence difficulties to the proximity of the solid phase and they most likely result from an artifact of the integral equation. On the other hand, the empirical Hansen–Verlet freezing rule[13] indicates that these limiting states are well within the fluid–solid coexistence region, in accordance with the phase diagram proposed by Likos *et al.*[6] Moreover, at least for the star polymer model potentials that present the logarithmic singularity at zero separation, it has been found that this empirical rule is valid.[14]

As to the high temperature and high packing fraction regime illustrated in Fig. 8, we observe first a tendency to adopt the ideal gas structure resulting from the decrease in size in the energy barrier that prevents multiple occupancy. As a consequence the structure of the fluid is smeared out and particles from the nearest neighbor shells move inside the particle core. This is further confirmed by the values of the average coordination number

$$n(r)=24\eta\int_0^r s^2 g(s)\,ds$$

also shown in Fig. 8. When the density is further increased, although the multiple occupancy of the core region rises even more [there are no longer values of $g(r)=0$ for $r<\sigma$], the fluid exhibits again certain structure in the first and second neighbor shells.

In Fig. 9 we have plotted the limits reached in our calculations, where states of higher packing fractions and lower t became unattainable. Although this might still be somewhat inconclusive, it seems that the penetrable sphere model does not have the type of fluid–solid phase diagram exhibited by the Gaussian core model, the latter presents a stable liquid phase for some densities higher than the solid and some type of critical temperature above which it is no longer possible to have a stable solid.[5]

Finally, in Figs. 10 and 11 we have presented the bridge

TABLE I. Thermodynamic properties obtained through various paths and optimized parameters in the ZSEP closure for a penetrable sphere fluid at packing fraction $\eta=0.3$. Here the quantity $\ln y_{zst}$ is calculated using Eq. (13) and $\beta P^a/\rho$ through Eq. (17). The meaning of the remaining subscripts and superscripts is explained in the text.

t	ζ	ϕ	α	σ_{wca}	ρ	ρ_{GD}	$1/\kappa_T^b$	$1/\kappa_T^v$	$\ln y(0)_{cr}$	$\ln y(0)_{zst}$	$\beta P^v/\rho$	$\beta P^a/\rho$	βa^{ex}	$\beta\mu_1$
0.1	1.274	1.013	1.016	0.983	0.573	0.597	10.56	10.57	4.843	4.833	4.029	3.598	1.804	4.833
0.2	0.742	0.966	0.973	0.980	0.573	0.584	8.39	8.39	4.472	4.473	3.760	3.603	1.8459	4.606
0.5	0.258	0.800	1.900	0.935	0.573	0.572	4.44	4.44	2.163	2.164	2.571	2.575	1.339	2.910
1.0	0.208	0.723	0.847	0.844	0.573	0.573	2.94	2.94	0.906	0.905	1.921	1.923	0.8536	1.775

TABLE II. Thermodynamic properties obtained through various paths and optimized parameters in the ZSEP closure for a penetrable sphere fluid at packing fraction $\eta=0.5$. Here the quantity $\ln y_{zst}$ is calculated using Eq. (13) and $\beta P^a/\rho$ through Eq. (17). The meaning of the remaining subscripts and superscripts is explained in the text.

t	ζ	ϕ	α	σ_{wca}	ρ	ρ_{GD}	$1/\kappa_T^b$	$1/\kappa_T^v$	$\ln y(0)_{cr}$	$\ln y(0)_{zst}$	$\beta P^v/\rho$	$\beta P^a/\rho$	βa^{ex}	$\beta\mu_1$
0.1	0.589	0.962	1.114	0.983	0.955	1.098	23.77	20.73	12.475	12.610	9.931	7.225	4.174	13.10
0.2	0.356	0.910	1.158	0.980	0.955	1.023	12.47	11.03	7.705	7.835	6.220	5.484	3.690	8.91
0.5	0.079	0.427	1.119	0.935	0.955	0.960	3.42	3.41	6.775	6.603	3.775	3.740	2.422	5.20
1.0	0.083	0.344	1.249	0.844	0.955	0.957	4.34	4.33	1.392	1.390	2.609	2.599	1.484	3.09

functions extracted from the simulation data using Verlet's extension procedure[15] for various thermodynamic states and compared with results from the ZSEP closure. We note that these extracted bridge functions are *not* direct MC results. Numerical treatment on the MC data was performed. We compare the ZSEP $B(r)$ with the MC-derived $B(r)$ in Figs. 10 and 11. There are visible discrepancies in the ZSEP results for $r<1.5$. These discrepancies correspond to the residual inconsistencies shown in Tables I and II. The sources of the discord are analyzed and attributed to: (1) the extension of the MC data has introduced inevitable numerical errors, derived from the finite ranges of the simulated data and their statistical scatter near zero-separation. (2) The ZSEP bridge function [Eq. (3)] contains three parameters. In the parameter space spanned by α,ϕ, and ζ, there is no guarantee that our search method has reached the global minimum for the residual inconsistencies. (3) The approximate assumption that the dimer-monomer bridge function [Eq. (14)] has the same parameters as the monomer–monomer values, while in fact they should have been different.[16]

We remark that in this particular incarnation of the ZSEP calculation, all that were used were self-consistencies, no extraneous information was needed. Two global conditions (thermodynamic-pressure consistency and Gibbs–Duhem relation) and one local condition (zero-separation theorem) were used to determine the three closure parameters: α, ϕ, and ζ. We took MC data only for comparison, not for the construction of the closures.

In summary, we have presented a viable theoretical approach to determine the structure and thermodynamics of the penetrable sphere model, and consequently suitable for any system with ultrasoft interactions. Since these types of materials are mostly often characterized by their polydispersity, a natural extension of this work would be the inclusion of polydispersity in the interactions (via the number of arms of the star copolymer and the particle size) by means of a treatment like the one proposed by Lado.[17] Work on this and related matters is planned.

ACKNOWLEDGMENTS

The authors thank Dr. C. N. Likos and M. Watzlawek for generously providing the yet unpublished computer simulation data presented herein and for illuminating comments. This work has been supported by the Spanish Direccion General de Enseñanza Superior e Investigación Científica under Grant No. PB97-0258-C02-02.

[1] C. N. Likos *et al.*, Phys. Rev. Lett. **80**, 4450 (1998).
[2] G. S. Grest *et al.*, Adv. Chem. Phys. **XCIV**, 67 (1996).
[3] M. Watzlawek, H. Löwen, and C. N. Likos, J. Phys.: Condens. Matter **10**, 8189 (1998).
[4] C. Marquest and T. A. Witten, J. Phys. (France) **50**, 1267 (1989).
[5] F. H. Stillinger and D. K. Stillinger, Physica A **244**, 358 (1997).
[6] C. N. Likos, M. Watzlawek, and H. Löwen, Phys. Rev. E **58**, 3135 (1999).
[7] L. L. Lee, J. Chem. Phys. **97**, 8606 (1992).
[8] L. L. Lee, D. Ghonasgi, and E. Lomba, J. Chem. Phys. **104**, 8058 (1996).
[9] L. L. Lee, J. Chem. Phys. **103**, 9388 (1995).
[10] E. Lomba and L. L. Lee, Int. J. Thermophys. **17**, 663 (1996).
[11] L. Verlet, Mol. Phys. **41**, 183 (1980).
[12] D. M. Duh and D. Henderson, J. Chem. Phys. **104**, 6472 (1996).
[13] J. P. Hansen and L. Verlet, Phys. Rev. **184**, 151 (1969).
[14] M. Watzlawek, C. N. Likos, and H. Löwen, Phys. Rev. Lett. **82**, 5289 (1999).
[15] L. Verlet, Phys. Rev. **165**, 202 (1968).
[16] L. L. Lee, J. Chem. Phys. **107**, 7360 (1997).
[17] F. Lado, Phys. Rev. E **54**, 4411 (1996).